Encapsulation of Cyclooctasulfur Molecules in an Open Metal–Sulfide Framework. Isolation of the Host–Guest Complex $Cs_2Sn_3S_7 \cdot {}^1/_2S_8$ from Molten Cesium Polysulfide Fluxes

Gregory A. Marking and Mercouri G. Kanatzidis*

Department of Chemistry, Michigan State University, East Lansing, Michigan 48824

Received April 21, 1995. Revised Manuscript Received July 13, 1995[⊗]

$Cs_2Sn_3S_7 \cdot {}^1/_2S_8$ was synthesized in 50–60% yield by reacting Sn with a Cs_2S_x flux at temperatures from 400 to 500 °C. The new greenish yellow ternary sulfide $Cs_2Sn_3S_7 \cdot {}^1/_2S_8$ crystallizes in the monoclinic $C2/c$ space group (No. 15) with $a = 22.350(6)$ Å, $b = 13.238(2)$ Å, $c = 16.301(4)$ Å, $\beta = 124.424(2)°$, $V = 3978.2(3.5)$ Å^3, $Z = 8$. $D_{calc} = 3.25$g/cm^3, number of data with $F_o^2 > 3\sigma(F_o^2)$ 3320, number of variables 182. The final $R/R_w = 3.8/4.9$. The structure of $Cs_2Sn_3S_7 \cdot {}^1/_2S_8$ consists of Sn_3S_4 defect cubane units connected by $(\mu\text{-}S)_2$ bridges forming large open rings in $Sn_3S_7^{2-}$ anionic layers. These layers are stacked along the c direction so that the open rings are aligned forming channels. Cs^+ cations are located between the layers and cyclooctasulfur molecules are found to statistically occupy overlapping conformations within the channels. Raman and vibrational spectroscopic data confirm the presence of the S_8 molecules. Single-crystal optical spectra indicate that this semiconductor has an indirect bandgap of 2.64 eV.

Introduction

The possibility of open metal chalcogenide framework structures that combine the utility of microporous oxides with the useful electronic properties of metal chalcogenides to form a new class of microporous chalcogenides is intriguing. Given the enormous utility of microporous oxides (such as zeolites) in chemical technology and the corresponding prominence of metal chalcogenides in electronic applications, it is worthwhile to envision materials that would combine the useful properties of both classes into one new class of microporous chalcogenides. Although such materials have not been reported to date, a few publications have made reference to this concept.[1,2] Bedard and co-workers reported the hydrothermal synthesis of several tin sulfides that display microporous activity after partial removal of the occluded template.[1] Another open chalcogenide framework was reported in the antimony sulfide system using the hydrothermal method.[2] Recently, a novel molten salt approach using $(Ph_4P)_2Se_x$ fluxes at 200 °C was shown to give $(Ph_4P)[M(Se_6)_2]$ (M = Ga, In, Tl).[3] The open polymeric framework in these compounds consists of tetrahedral M^{3+} centers and bridging Se_6^{2-} ligands that form an extended structure in two dimensions with Ph_4P^+ cations residing within the layers.

During exploratory investigations on the reactivity of tin in molten alkali polychalcogenides, some results of which have already been published in detail,[4] we discovered an unusual compound with an open tin–sulfide framework which encapsulates a molecule of elemental sulfur. We report here the synthesis and characterization of $Cs_2Sn_3S_7 \cdot {}^1/_2S_8$. The structure of this new compound is nearly isomorphous to that of $Cs_2Sn_3Se_7$[5] but with inclusion of elemental S_8 into the channels found within the structure. The sulfur analogue, $Cs_2Sn_3S_7$ without the inserted S_8 rings, is so far unknown, but $[enH_2][Sn_3S_7] \cdot {}^1/_2en$,[6] $[NMe_4]_2 \cdot Sn_3S_7 \cdot H_2O$,[7] and TEA-SnS-1[8] have closely related structures. A growing number of similar open-framework structures based on $Sn_4S_9^{2-}$ anionic layers have also been reported.[9,10] On the other hand, a rubidium compound of analogous stoichiometry, $Rb_2Sn_3S_7 \cdot 2H_2O$, has a completely different structure.[11]

$Cs_2Sn_3S_7 \cdot {}^1/_2S_8$ is novel in both synthesis and structure. The synthetic conditions used to prepare this compound are drastically different from the hydrothermal and methanothermal conditions used to prepare the compounds mentioned above which contain similar $Sn_3S_7^{2-}$, $Sn_3Se_7^{2-}$, and $Sn_4S_9^{2-}$ anionic sheets. The inclusion of elemental S_8 rings into channels within a structure is

[⊗] Abstract published in *Advance ACS Abstracts,* September 1, 1995.

(1) (a) Bedard, R. L.; Wilson, S. T.; Vail, L. D.; Bennett, E. M.; Flanigen, E. M. *Zeolites: Facts, Figures, Future,* Jacobs, P. A., van Santen, R. A., Eds.; Elsevier Science Publishers B. V.:Amsterdam, The Netherlands, 1989, pp 375–387. (b) Bedard, R. L.; Vail, L. D.; Wilson, S.T.; Flanigen, E. M. *U.S. Patent 4,880,761,* 1989.

(2) Parise, J. B. *Science* **1991,** *251,* 293–294.

(3) Dhingra, S.; Kanatzidis, M. G. *Science* **1992,** *258,* 1769–1772.

(4) Sheldrick, W. S.; Braunbeck, H.-G. *Z. Naturforsch.* **1990,** *45B,* 1643–1646.

(5) Liao, J.-H.; Varotsis, C.; Kanatzidis, M. G. *Inorg. Chem.* **1993,** *32,* 2453–2462.

(6) Sheldrick, W. S.; Braunbeck, H.-G. *Z. Anorg. Allg. Chem.* **1993,** *619* , 1300–1306.

(7) Parise, J. B.; Ko, Y,; Rijssenbeek, J.; Nellis, D. M.; Tan, K.; Koch, S. *J. Chem. Soc., Chem. Commun.* 1994, 527.

(8) Enzel, P.; Henderson, G. S.; Ozin, G. A.; Bedard, R. L. *Adv. Mater.* **1995,** *7,* 166–170.

(9) (a) Enzel, P.; Henderson, G. S.; Ozin, G. A.; Bedard, R. L. *Adv. Mater.* **1995,** *7,* 64–68. (b) Jiang, T.; Lough, A. J.; Ozin, G. A.; Young, D. *Chem. Mater.* **1995,** *7,* 245–248.

(10) Ko, Y.; Tan, K.; Nellis, D. M.; Koch, S.; Parise, J. B. *J. Solid State Chem.* **1995,** *114,* 506–511.

(11) Sheldrick, W. S.; Schaaf, B. *Z. Anorg. Allg. Chem.* **1994,** *620,* 1041–1045.

0897-4756/95/2807-1915$09.00/0

unusual. In what appears to us to be the only other example, the crystal structure of a sulfur sorption complex of zeolite A has been reported with S_8 molecules located inside the zeolite cavities.[12] Related chemistry includes cocrystallization of S_8 rings with other molecular species, such as CHI_3 and SbI_3 (forming $CHI_3{\cdot}3S_8$[13] and $SbI_3{\cdot}3S_8$,[14] respectively) which has been known since the early 1960s. Since then, other compounds containing similar "lattice" S_8 have also been reported. Chains of Se and Te have been injected into matrixes of the zeolite mordenite and characterized using Raman spectroscopy[15] and Se chains in the channels of mordenite have been structurally characterized using X-ray Rietveld refinement techniques.[16] The interesting phase $Ta_4P_4S_{29}$[17] which contains polymeric sulfur within its channels has been reported. Recently, a Te_8 ring was found in the compound Cs_3Te_{22}.[18]

Experimental Section

Synthesis. All manipulations were carried out under a nitrogen atmosphere. Reagents were used as obtained: (i) Sn metal, 99.8%, −325 mesh, Cerac, Milwaukee, WI; (ii) sulfur powder, sublimed, Mallinckrodt, Paris, KY; (iii) cesium metal, 99.98%, Cerac, Milwaukee, WI. Cs_2S was prepared as described earlier.[4]

Large (up to ~3 mm^3) high-quality crystals of $Cs_2Sn_3S_7{\cdot}^1/_2S_8$ can be synthesized in 50−60% yield through the reactive flux technique at temperatures from 400−500 °C. The crystals can range in color from yellow with a slight green tint to bright yellow-green. A typical synthesis follows: A mixture of Sn metal, previously prepared Cs_2S, and elemental sulfur in the molar ratios 2:2:18 was loaded into a ~10 mL Pyrex tube in an N_2 glovebox. The tube was evacuated to a residual pressure of $<10^{-3}$ Torr and flame-sealed. The mixture was heated to 400 °C over 16 h, isothermed at that temperature for 5 days, and cooled to 180 °C at −4 °C/h. The product was washed with DMF to remove excess Cs_2S_x flux. A brief wash with CS_2 was used to remove any unreacted sulfur from the product. Methanol, acetone, and diethyl ether were successively used to rinse and dry the product. The yield for this specific reaction was 58% based on Sn. The product is stable in water and other common solvents, and no decomposition was detected in samples left under ambient atmospheric conditions for periods exceeding 3 months.

The product visually appeared to be homogeneous, and comparison of the calculated and experimental X-ray powder diffraction patterns confirmed the homogeneity. Semiquantitative SEM-EDS analysis resulted in the average formulation $Cs_{1.16}Sn_{2.74}S_{11}$ for these green-yellow crystals, which is in good agreement with the stoichiometry determined through an X-ray single-crystal study. In our laboratory this analytical technique generally results in low values for the cesium content of known materials with similar stoichiometries.

Physical Measurements. Raman spectra were recorded using a BIO-RAD FT Raman spectrometer with a Spectra-Physics Topaz T10-106c laser. FT-IR spectra for this compound were recorded on solids in a CsI matrix. Data were recorded from the far-IR region (650-100 cm^{-1}, 4 cm^{-1} resolution) with the use of a Nicolet 740 FT-IR spectrometer equipped with a TGS/PE detector and beam splitter. Semiquantitative microprobe analysis were performed with a JEOL JSM-6400V scanning electron microscope (SEM) equipped with a Tracor Northern energy-dispersive spectroscope (EDS) detector. Data acquisitions were performed using an accelerating voltage of 20 kV and a 30 s accumulation time. Powder X-ray diffraction (XRD) was performed using a calibrated Phillips XRD-3000 controlled by a PDP 11 computer using Ni-filtered Cu radiation and operating at 40 kV and 20 mA. Calculated X-ray powder patterns used for comparative purposes were obtained using Cerius[2] software.[19]

Optical diffuse reflectance measurements were made at room temperature with a Shimadzu UV-3101PC double-beam, double-monochromator spectrophotometer operating in the 200−2500 nm region. The instrument was equipped with an integrating sphere and controlled by a personal computer. $BaSO_4$ powder was used as a reference (100% reflectance) and absorption data were calculated from reflectance data using the Kubelka−Munk function.[20] Optical transmission measurements were made at room temperature on single crystals using a Hitachi U-6000 microscopic FT spectrophotometer with an Olympus BH-2 metallurgical microscope over a range from 380 to 900 nm.

Differential thermal analyses (DTA) were performed using a computer-controlled Shimadzu DTA-50 thermal analyzer. Amounts of 10−20 mg of sample were sealed in quartz tubes under vacuum and then heated at 10 °C/min to temperatures ranging from 300 to 600 °C, isothermed from 10 to 20 min, and finally cooled to 100 °C at 10 °C/min. Empty sealed quartz tubes of approximately the same mass as the sample tubes were present on the reference side of the detector during measurements. Thermogravimetric analysis was performed using a computer-controlled Shimadzu TGA-50 thermogravimetric analyzer. Sample quantities of 10−20 mg were placed in small quartz buckets and heated in a flowing nitrogen atmosphere at rates ranging from 5 to 0.5 °C/min. The DTA and TGA samples were examined by powder X-ray diffraction, Raman spectroscopy, and SEM-EDS analysis after the experiments.

X-ray Crystallography. A single crystal with regular shape was mounted on a glass fiber, and an intensity data set was collected using a Rigaku AFC6S diffractometer with graphite monochromated Mo Kα radiation operating at 50 kV and 30 mA at room temperature. Three standard reflections were monitored every 600 reflections and indicated that no significant decay occurred. Unique data (h, k, $+l$ and h, k, $-l$) were collected out to 55° in 2θ using ω-2θ scans. The diffraction data were processed and the structure was refined using TEXSAN software.[21] All atoms except those in the S_8 molecules were found using direct methods (SHELXS-86)[22] and the remaining sulfur atoms were found through the difference Fourier technique. The data collected at >40° in 2θ were essential in resolving the correct placement of the S_8 molecules which were found to statistically occupy two overlapping symmetrically equivalent conformations.

An empirical absorption correction based on ψ-scans was applied to the data, and equivalent data were averaged. After complete anisotropic refinement, the R and R_w were 4.1% and 5.1%, respectively. When an additional DIFABS[23] absorption correction was applied during refinement, the final R and R_w dropped to 3.8% and 4.9%. The esd's for the atomic positions,

(12) Seff, K. *J. Phys. Chem.* **1972**, *76*, 2601−2605.
(13) Bjorvatten, T. *Acta Chem. Scand.* **1962**, *16*, 749−754.
(14) Bjorvatten, T.; Hassel, O.; Lindheim, A. *Acta Chem. Scand.* **1963**, *17*, 689−702.
(15) Bogomolov, V. N.; Poborchy, V. V.; Romanov, S. G.; Shagin, S. I. *J. Phys. C: Solid State Phys.* **1985**, *18*, L313-L317.
(16) Terasaki, O.; Shiokawa, K.; Ito, M.; Watanabe, D.; Thomas, J. M. In *Zeolites: Facts, Figures, Future*, Jacobs, P. A., van Santen, R. A., Eds.; Elsevier Science Publishers B. V.: Amsterdam, The Netherlands, 1989; pp 431−438.
(17) Evain, M.; Queignec, M.; Brec, R.; Rouxel, J. *J. Solid State Chem.* **1985**, *56*, 148−157.
(18) Sheldrick, W. S.; Wachhold M. *Angew. Chem., Int. Ed. Engl.* **1995**, *34*, 450−452
(19) CERIUS[2], Version 1.6, Molecular Simulations Inc., Cambridge, England, 1994.
(20) (a) Wendlandt, W. W.; Hecht, H. G. *Reflectance Spectroscopy*; Interscience Publishers: New York, 1966. (b) Kotüm, G. *Reflectance Spectroscopy*; Springer Verlag: New York, 1969. (c) Tandon, S. P.; Gupta, J. P. *Phys. Status Solidi* **1970**, *38*, 363−367.
(21) TEXSAN-TEXRAY Structure Analysis Package, Molecular Structure Corp., The Woodlands, TX, 1985.
(22) Sheldrick, G. M. In *Crystallographic Computing 3*, Sheldrick, G. M., Kruger, C., Goddard, R., Eds.; Oxford University Press: Oxford, U.K., 1985, pp 175−189.
(23) DIFABS: Walker, N.; Stuart, D. DIFABS: An Empirical Method for Correcting Diffraction Data for Absorption Effects. *Acta Crystallogr.* **1983**, *A39*, 158−166.

Table 1. Crystal Data for $Cs_2Sn_3S_7{}^1/_2S_8$

formula	$Cs_2Sn_3S_7{}^1/_2S_8$
fw	974.54
a, Å	22.350(6)
b, Å	13.238(2)
c, Å	16.301(4)
α (deg)	90.0
β (deg)	124.424(8)
γ (deg)	90.0
Z, V (Å^3)	8, 3978(3)
space group	$C2/c$ (No. 15)
d_{calc} (g/cm^3)	3.254
crystal size, mm	0.23 × 0.26 × 0.28
temp (°C)	23
radiation	Mo Kα
μ (Mo Kα), cm^{-1}	84.30
secondary ext coeff (10^{-7})	0.69 (5)
scan mode	$2\theta-\omega$
scan speed (deg/min)	4
2θ max, deg	55
no. of data collected	4909
no. of unique data	4778
no. of data observed, $I > 3\sigma(I)$	3320
no. of variables	182
absorption correction	ψ scans/DIFABS
ψ scan abs ratio (min/max)	0.6976
R/R_w (%)	3.84/4.90
GOF	1.73
residual e$^-$ density (pos)	+1.860
residual e$^-$ density (neg)	−1.332

[a] $R = \Sigma(|F_o| - |F_c|)/\Sigma|F_o|$, $R_w = \{\Sigma w(|F_o| - |F_c|)^2/\Sigma w|F_o|^2\}^{1/2}$.

Table 2. Positional Parameters and B_{eq}'s for $Cs_2Sn_3S_7{}^1/_2S_8$

atom	x	y	z	B_{eq}
Cs(1)	0.01651(4)	0.18400(5)	0.97703(6)	3.63(3)
Cs(2)	0.26535(6)	0.03963(8)	0.57255(7)	5.98(4)
Sn(1)	0.08313(3)	0.03050(5)	0.26664(5)	1.92(2)
Sn(2)	0.20896(3)	0.85667(5)	0.27040(5)	2.23(2)
Sn(3)	0.23405(3)	0.12874(5)	0.26927(5)	2.24(2)
S(1)	0.0389(1)	0.0462(2)	0.3784(2)	2.48(8)
S(2)	0.1660(1)	0.1739(2)	0.3394(2)	2.80(9)
S(3)	0.1385(1)	0.8669(2)	0.3411(2)	2.9(1)
S(4)	0.1283(1)	0.0043(2)	0.1510(2)	2.10(7)
S(5)	0.1705(1)	0.7582(2)	0.1232(2)	3.1(1)
S(6)	0.2871(1)	0.7113(2)	0.3767(2)	3.1(1)
S(7)	0.3099(1)	0.9786(2)	0.3413(2)	3.4(1)
S(8)	0.9561(6)	0.3289(7)	0.130(1)	7.1(4)
S(9)	0.010(1)	0.3080(6)	0.2786(9)	6.6(6)
S(10)	0.9500(5)	0.3742(8)	0.3213(7)	6.4(4)
S(11)	0.9982(5)	0.511(1)	0.3837(7)	6.5(4)
S(12)	0.9468(7)	0.6208(7)	0.2829(7)	7.7(5)
S(13)	0.9953(7)	0.6457(6)	0.2134(8)	6.9(4)
S(14)	0.9449(8)	0.5705(8)	0.0872(8)	9.1(6)
S(15)	0.9998(8)	0.4430(8)	0.102(1)	7.6(5)

thermal parameters, and bond distances and angles were also slightly improved. After the structure was completely refined, it was found that an alternate setting for C-centered monoclinic unit cells facilitated description of the structure and production of ORTEP diagrams. The structure is reported here using this alternate setting. Tables 1 and 2 contain pertinent crystallographic data, results, and atomic parameters. The thermal parameters listed in Table 2 for S(8) through S(15), atoms of the two statistically occupied cyclooctasulfur conformations, are significantly larger than the thermal parameters of the other sulfur positions. The thermal parameters of these sulfur atoms correlate with their freedom of movement (they are bonded only to each other) and to their disordered site occupancies.

Results and Discussion

Structure. $Cs_2Sn_3S_7{}^1/_2S_8$ has a 2-dimensional solid-state framework consisting of anionic $Sn_3S_7{}^{2-}$ layers parallel to the ab plane with Cs^+ cations located between the layers (Figure 1). These layers consist of large interconnected rings and are stacked (offset by ~9 Å along the a-axis) so that the rings are aligned forming large open channels along the c axial direction. The shortest sulfur−sulfur distance across the channels is 10.47 Å but the Cs^+ cations also partially obstruct the openings having a shortest Cs^+-Cs^+ distance across the channel openings of 8.47 Å. Neutral S_8 molecules are located in these channels (Figure 2). The $Sn_3S_7{}^{2-}$ layers are built up from SnS_5 trigonal bipyramidal units. Every three SnS_5 units are fused into larger Sn_3S_{10} units by sharing edges with one S atom being the common axial S for all three SnS_5 trigonal bipyramids. The Sn_3S_4 cores of these Sn_3S_{10} units can be viewed as defect cubanes with one Sn center missing. One Sn_3S_{10} unit is shown in Figure 3 with the individual Sn and S atoms labeled. The Sn_3S_{10} units are further connected by sharing their terminal sulfurs. Alternatively, the layers can be viewed as being built from Sn_3S_4 defect cubane cores, which are linked to three other cores by $(\mu$-S$)_2$ bridges. Table 3 contains most of the interatomic distances <3.7 Å for this structure but only the sulfur−sulfur bonding distances in the S_8 rings are included. The interatomic bond angles found in a defect cubane Sn_3S_{10} unit and in a cyclooctasulfur molecule, as well as the S_8 torsion angles, are listed in Table 4.

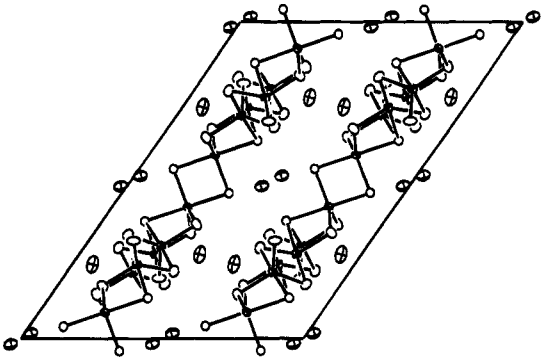

Figure 1. Projection down the b axis of $Cs_2Sn_3S_7{}^1/_2S_8$ showing only the anionic $Sn_3S_7{}^{2-}$ layers and the Cs^+ cations. Ellipsoids with shaded octants represent Sn, crossed ellipsoids represent Cs^+ cations, and open ellipsoids represent sulfur. All ellipsoids are drawn to 50% probability.

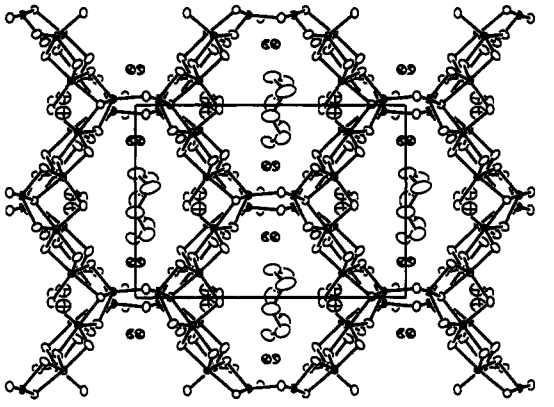

Figure 2. Projection down the c axis of $Cs_2Sn_3S_7{}^1/_2S_8$ showing the channels and the S_8 molecules. Ellipsoids with shaded octants represent Sn, crossed ellipsoids represent Cs^+ cations, and open ellipsoids represent sulfur. Ellipsoids are drawn to 50% probability, and only one conformation is shown for the S_8 molecules.

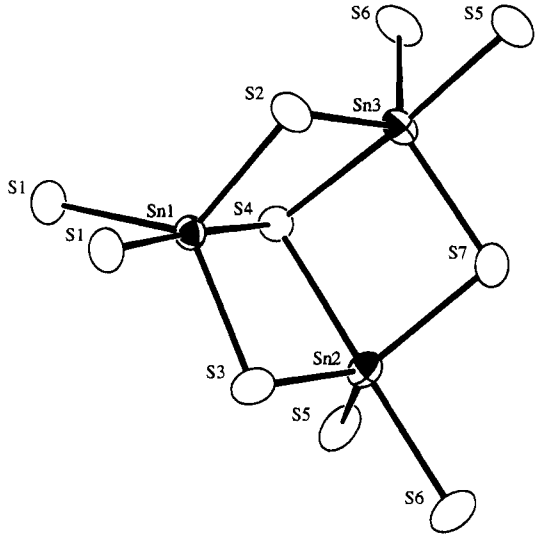

Figure 3. A defect cubane Sn_3S_{10} cluster unit with individual atom labels. The atoms are represented by 50% thermal ellipsoids.

Table 3. Interatomic Distances <3.7 Å for $Cs_2Sn_3S_7{}^1/_2S_8$ Including only Sulfur–Sulfur Bonding Distances within the S_8 Ring

atoms	distance	atoms	distance
Cs(1)–S(1)	3.610(3)	S(1)–S(1)	3.509(5)
Cs(1)–S(4)	3.455(2)	S(1)–S(2)	3.657(4)
Cs(1)–S(4)	3.661(2)	S(1)–S(3)	3.533(4)
Cs(1)–S(5)	3.606(3)	S(1)–S(4)	3.531(3)
Cs(1)–S(6)	3.641(3)	S(2)–S(4)	3.501(3)
Cs(1)–S(12)	3.681(9)	S(2)–S(5)	3.530(4)
Cs(1)–S(14)	3.664(9)	S(2)–S(8)	3.67(1)
Cs(2)–S(2)	3.604(3)	S(2)–S(9)	3.52(1)
Sn(1)–Sn(1)	3.439(2)	S(2)–S(10)	3.60(1)
Sn(1)–Sn(2)	3.607(1)	S(3)–S(4)	3.488(3)
Sn(1)–Sn(3)	3.593(1)	S(3)–S(6)	3.665(4)
Sn(1)–S(1)	2.525(3)	S(4)–S(5)	3.491(4)
Sn(1)–S(1)	2.404(3)	S(4)–S(6)	3.502(3)
Sn(1)–S(2)	2.440(3)	S(4)–S(7)	3.461(4)
Sn(1)–S(3)	2.448(3)	S(5)–S(6)	3.476(4)
Sn(1)–S(4)	2.616(2)	S(5)–S(8)	3.63(1)
Sn(2)–Sn(3)	3.647(1)	S(6)–S(7)	3.667(4)
Sn(2)–Sn(3)	3.475(1)	S(7)–S(10)	3.602(9)
Sn(2)–S(3)	2.426(3)	S(7)–S(14)	3.45(1)
Sn(2)–S(4)	2.625(2)		
Sn(2)–S(5)	2.421(3)	S(8)–S(9)	2.03(2)
Sn(2)–S(6)	2.517(3)	S(9)–S(10)	2.03(2)
Sn(2)–S(7)	2.466(3)	S(10)–S(11)	2.06(2)
Sn(3)–S(2)	2.439(3)	S(11)–S(12)	1.99(2)
Sn(3)–S(4)	2.621(2)	S(12)–S(13)	1.99(2)
Sn(3)–S(5)	2.517(3)	S(13)–S(14)	1.97(1)
Sn(3)–S(6)	2.411(3)	S(14)–S(15)	2.02(2)
Sn(3)–S(7)	2.440(3)	S(15)–S(8)	1.99(1)

The S_8 molecules found in the open channels are slightly distorted from the ideal S_8 geometry having slightly short but reasonable bond distances (1.97–2.06 Å), and reasonable bond and torsion angles (106.6–110.5° and 93.4–101.2°, respectively). For comparison, α-S_8[24] has sulfur–sulfur distances of 2.046–2.052 Å, bond angles from 107.3 to 109.0°, and torsion angles of 98.5°. The distortion of the S_8 molecules found in the zeolite A (S–S bond lengths 1.94(8) Å, bond angles averaging 123(6)°, and dihedral angles 72°) is larger than that found here and is explained as resulting from close contacts with the surrounding Na^+ ions.[12]

(24) Coppens, P.;Yang, Y. W.; Blessing, R. H.; Cooper, W. F.; Larsen, F. K. *J. Am. Chem. Soc.* **1977**, *99*, 760–766.

Table 4. Intermolecular Bond Angles for the Sn_3S_{10} Defect Cubane Unit, Intermolecular Bond Angles, and Torsion Angles for the Cyclooctasulfur

atoms	angle (deg)	atoms	angl (deg)
S(1)–Sn(1)–S(1)	90.74(9)	S(6)–Sn(3)–S(7)	122.6(1)
S(1)–Sn(1)–S(2)	94.84(9)	Sn(1)–S(1)–Sn(1)	88.44(8)
S(1)–Sn(1)–S(3)	90.52(9)	Sn(1)–S(2)–Sn(3)	94.85(9)
S(1)–Sn(1)–S(4)	177.08(8)	Sn(1)–S(3)–Sn(2)	95.49(9)
S(1)–Sn(1)–S(2)	122.56(9)	Sn(1)–S(4)–Sn(2)	87.00(7)
S(1)–Sn(1)–S(3)	122.6(1)	Sn(1)–S(4)–Sn(3)	86.64(7)
S(1)–Sn(1)–S(4)	89.32(8)	Sn(2)–S(4)–Sn(3)	88.09(7)
S(2)–Sn(1)–S(3)	114.5(1)	Sn(2)–S(5)–Sn(3)	89.44(9)
S(2)–Sn(1)–S(4)	87.58(8)	Sn(2)–S(6)–Sn(3)	89.67(9)
S(3)–Sn(1)–S(4)	86.99(8)	Sn(2)–S(7)–Sn(3)	96.04(9)
S(3)–Sn(2)–S(4)	87.25(8)		
S(3)–Sn(2)–S(5)	122.6(1)	S(8)–S(9)–S(10)	106.8(9)
S(3)–Sn(2)–S(6)	95.71(9)	S(9)–S(10)–S(11)	106.6(6)
S(3)–Sn(2)–S(7)	114.1(1)	S(10)–S(11)–S(12)	109.6(6)
S(4)–Sn(2)–S(5)	87.46(8)	S(11)–S(12)–S(13)	110.0(7)
S(4)–Sn(2)–S(6)	176.55(8)	S(12)–S(13)–S(14)	109.6(7)
S(4)–Sn(2)–S(7)	85.60(9)	S(13)–S(14)–S(15)	110.5(8)
S(5)–Sn(2)–S(6)	89.46(9)	S(14)–S(15)–S(8)	108.4(7)
S(5)–Sn(2)–S(7)	122.3(1)	S(15)–S(8)–S(9)	110.0(8)
S(6)–Sn(2)–S(7)	94.8(1)		
S(2)–Sn(3)–S(4)	87.51(8)	S(8)–S(9)–S(10)–S(11)	101.2(8)
S(2)–Sn(3)–S(5)	90.84(9)	S(9)–S(10)–S(11)–S(12)	97.7(7)
S(2)–Sn(3)–S(6)	121.7(1)	S(10)–S(11)–S(12)–S(13)	93.4(7)
S(2)–Sn(3)–S(7)	115.0(1)	S(11)–S(12)–S(13)–S(14)	96.6(9)
S(4)–Sn(3)–S(5)	176.02(9)	S(12)–S(13)–S(14)–S(15)	101.0(9)
S(4)–Sn(3)–S(6)	88.11(8)	S(13)–S(14)–S(15)–S(8)	96.4(8)
S(4)–Sn(3)–S(7)	86.22(8)	S(14)–S(15)–S(8)–S(9)	94(1)
S(5)–Sn(3)–S(6)	89.68(9)	S(15)–S(8)–S(9)–S(10)	100.2(9)
S(5)–Sn(3)–S(7)	97.8(1)		

The slightly distorted S_8 molecules found in $Cs_2Sn_3S_7{}^1/_2S_8$ have only nonbonding interactions with the rest of the structure as indicated from the shortest interatomic distances between the sulfur atoms of the S_8 rings and the Sn, Cs, and S atoms in the rest of the structure which include Sn(1)–S(9) 4.07(1) Å, Cs(1)–S(14) 3.664(9) Å, and S(7)–S(14) 3.45(1) Å. Two symmetrically related conformations exist for the S_8 molecules, each of which must be equally occupied in order to maintain the long-range order found in the space group $C2/c$. Each conformation can be no more than one-half occupied because both occupy the same region of space and the refinement gave no indication for less than one-half occupancy. One S_8 molecule is shown in Figure 4.

The origin of the unusual greenish coloration of these crystals has not been determined. The green color may result from the presence of S_5^+ radical ions which are reported to be blue.[25] Electron paramagnetic resonance spectroscopy (EPR) of this compound showed no meaningful signal. Another more likely possibility may be the presence of other sulfur rings such as S_7 or S_6 which absorb at slightly different wavelengths than does S_8.

Vibrational Spectroscopy. The Raman spectra for $Cs_2Sn_3S_7{}^1/_2S_8$ and α-S_8 (standard supplied by Bio-Rad) are shown in Figure 5A,B, respectively. The peaks seen in the spectra of α-S_8 agree well with literature values.[26] The peaks at 360, 336, and 285 cm^{-1} in Figure 5A are in the range of Sn–S vibrations. Comparison of the remaining peaks in Figure 5A and the peaks from α-S_8 in Figure 5B show good agreement in both peak posi-

(25) (a) Passmore, J.; Sutherland, G.; Taylor, P.; Whidden, T. K.; White, P. S. *Inorg. Chem.* **1981**, *20*, 3839–3845. (b) Burns, R. C.; Gillespie, R. J.; Sawyer, J. F. *Inorg. Chem.* **1980**, *19*, 1423–1432.

(26) Gautier, G.; Debeau, M. *Spectrochim. Acta* **1976**, *A32*, 1007–1010.

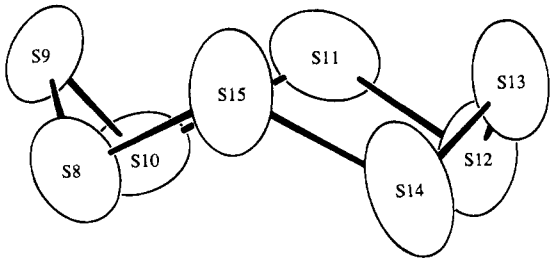

Figure 4. One of the two half-occupied symmetry related S_8 ring conformations found within the channels of $Cs_2Sn_3S_7 \cdot {}^1/_2S_8$. The sulfur atoms are labeled and drawn as 50% thermal ellipsoids.

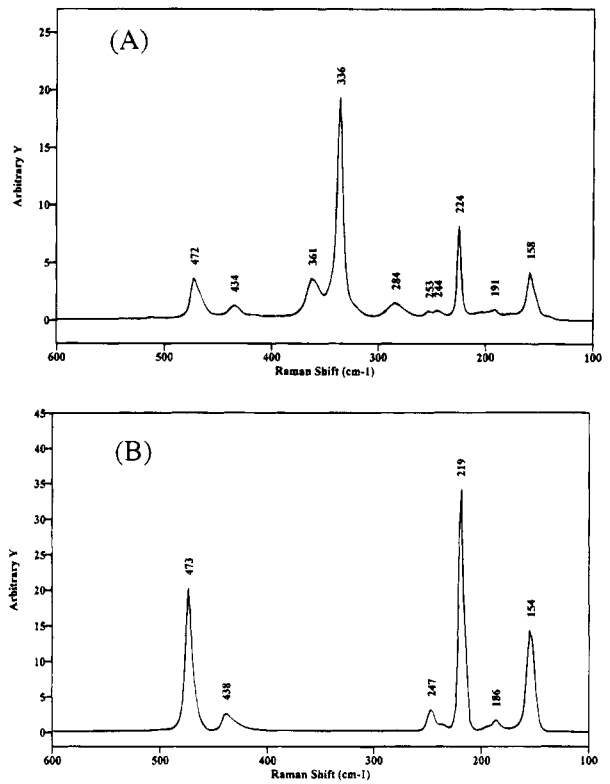

Figure 5. Raman spectra from the far-IR region, 600–100 cm^{-1} (A) $Cs_2Sn_3S_7 \cdot {}^1/_2S_8$, 2 cm^{-1} resolution; (B) cyclooctasulfur, S_8, 4 cm^{-1} resolution.

tions and relative intensities, strongly corroborating our crystallographic results.

The far-IR spectra of $Cs_2Sn_3S_7 \cdot {}^1/_2S_8$ also indicated the presence of a sulfur–sulfur bonded species consistent with rhombic α-S_8. Weak absorptions around 450–470 cm^{-1} in the range of S–S stretching were detected.

Optical Spectroscopy. The transparent greenish-yellow crystals of $Cs_2Sn_3S_7 \cdot {}^1/_2S_8$, when ground, result in an orange powder which gives optical diffuse reflectance spectra with severe tailing and without a steep absorption edge (~2.6 eV). The spectrum resulting from small unground crystals (<100 μm diameter) had less tailing and a steeper absorption edge at slightly higher energy, 2.62 eV. An optical transmission spectrum collected from a single crystal and converted to absorption data is shown in Figure 6. The absorption edge is much steeper than that found from the reflectance data and at a similar energy. The single crystal spectrum represents the bulk optical properties of $Cs_2Sn_3S_7 \cdot {}^1/_2S_8$, and it was used to evaluate the nature of the bandgap. The absorption$^{1/2}$ vs energy plot (Figure 7A) is very

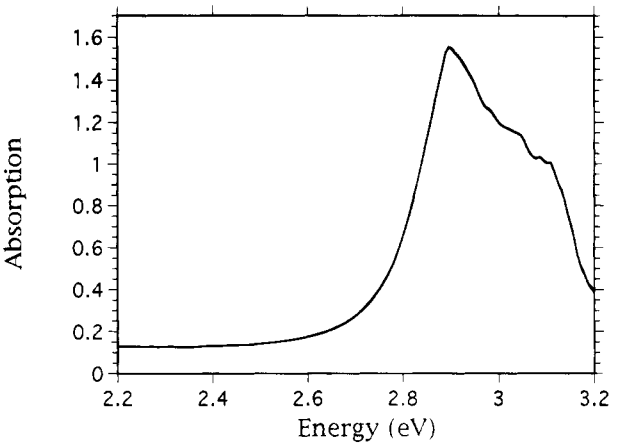

Figure 6. Single-crystal optical transmission data converted to absorption data for $Cs_2Sn_3S_7 \cdot {}^1/_2S_8$ and plotted as absorption vs energy.

nearly linear (goodness of fit 0.997) while the plot of absorption^2 vs energy (Figure 7B), significantly deviates from linearity (goodness of fit 0.957). A linear relationship between absorption$^{1/2}$ and energy is found in materials with indirect bandgaps,[27] and thus we conclude that $Cs_2Sn_3S_7 \cdot {}^1/_2S_8$ has an indirect bandgap. Independent experimental and theoretical evidence is needed to corroborate this conclusion. The transition responsible for this 2.64 eV bandgap is probably charge transfer in character from the primarily S-based valence band to the primarily Sn-based conduction band of the $[Sn_3S_7]^{2-}$ framework. It is unclear whether the guest molecule of sulfur is playing a role. The presence of an optical gap and the electron-precise nature of the compound confirms that we are dealing with a semiconductor.

Thermal Analysis. Differential thermal analysis, DTA, and thermogravimetric analysis, TGA, were used to characterize $Cs_2Sn_3S_7 \cdot {}^1/_2S_8$. The transparent green-yellow crystals were ground to a fine orange powder before use in these thermal analysis techniques.

When a sample was heated at +10 °C/min to 300 °C and cooled at −10 °C/min to 100 °C in the DTA, no endothermic or exothermic peaks could be detected above the background, but volatilized sulfur could visually be detected in the sample container away from the sample. Using the same heating and cooling rates to a maximum of 500 °C resulted in a melting endotherm at 436 °C and a broad cooling exotherm centered at 291 °C on the first cycle. The second and third cycles showed two endotherms at 414 and 432 °C upon heating, indicating that this compound does not melt congruently, and the same broad exotherm at 291 °C upon cooling. The X-ray powder diffraction pattern of the DTA residue was indexed as consisting primarily of $Cs_2Sn_2S_6$[4] and $Cs_2Sn_4S_9$[28] phases, but the volatilized sulfur contained in the closed sample container complicated characterization of this residue by Raman spectroscopy. SEM-EDS analysis confirmed the presence of two phases in the DTA residue having the approximate compositions $Cs_{1.2}Sn_2S_{7.0}$ and $Cs_{1.5}Sn_4S_{9.0}$, which are close to the compositions of the phases identified through powder XRD.

(27) (a) Pankove, J. I. *Optical Processes in Semiconductors;* Dover Publications, Inc.: New York, 1971, pp 34–42.
(28) Marking, G. A.; Kanatzidis, M. G., manuscript in preparation.

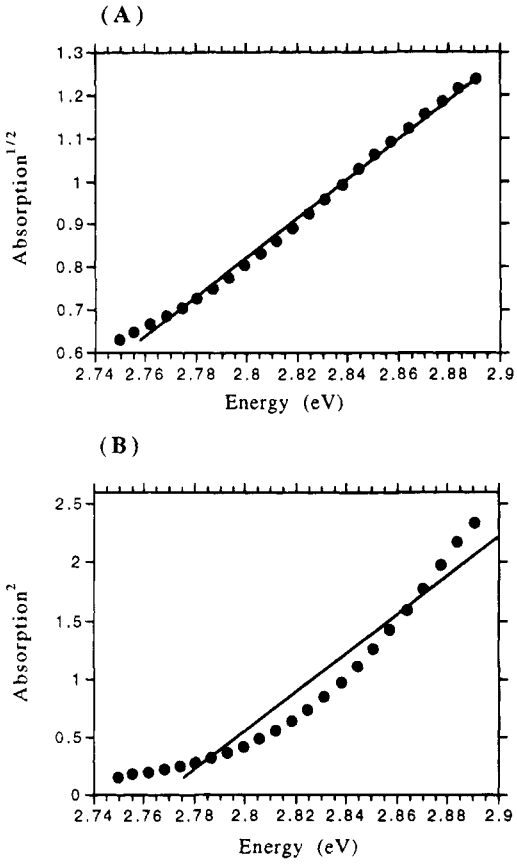

Figure 7. Single-crystal optical transmission data converted to absorption data for $Cs_2Sn_3S_7{\cdot}^1/_2S_8$. The region close to the absorption edge is plotted for (A) absorption$^{1/2}$ vs energy and (B) absorption^2 vs energy.

TGA experiments were also performed on finely ground samples under flowing nitrogen. When a sample was heated to 360 °C at a heating rate of +5 °C/min and held at that temperature for 1 h, a weight loss was observed beginning around 200 °C which increased to a 3% weight loss as 360 °C was reached and ended with an 11.06% total weight loss, corresponding to 84% loss of the S_8 molecules, after 1 h at 360 °C. Less than a 0.02% weight loss was observed over the last 20 min. Another sample was heated at a rate of +5 °C/min to 300 °C, then at a rate of +1 °C/min to 360 °C, and finally at a rate of +0.5 °C/min to 385 °C resulting in an 11.85% total weight loss, corresponding to 90% loss of the S_8, with almost no weight loss observed after 365 °C had been reached. Neither sample melted in these TGA experiments. X-ray powder diffraction patterns of both yellow powder TGA residues were indexed as resulting from mixtures of the $Cs_2Sn_2S_6$[4] and $Cs_2Sn_4S_9$ phases. Raman spectra of both TGA residues were also identified as resulting from mixtures of the $Cs_2Sn_2S_6$ and $Cs_2Sn_4S_9$ phases. The experimental weight losses (11.06 and 11.85% total weight loss) agree well with the calculated weight loss if it is assumed that seven sulfurs out of each S_8 are volatilized (11.52% total weight loss). A balanced chemical reaction can be used to describe the TGA experiments:

$$2Cs_2Sn_3S_7{\cdot}^1/_2S_8 \rightarrow Cs_2Sn_2S_6 + Cs_2Sn_4S_9 + 7S$$

Chemical Desulfurization and Ion Exchange. For this material to exhibit microporosity, the sulfur molecules and/or the Cs^+ cations must be removable or exchangeable. As seen above, the cyclooctasulfur molecules cannot be thermally removed from the channels of $Cs_2Sn_3S_7{\cdot}^1/_2S_8$ without changing the phase identity of the material. A variety of "soft" chemical methods of sulfur removal, based on the solubility and redox properties of sulfur, were attempted. Powder XRD, Raman spectroscopy, and SEM-EDS were used to characterize the resulting samples.

Small crystals of $Cs_2Sn_3S_7{\cdot}^1/_2S_8$ and ground powder were leached in carbon disulfide for 3 days, ethylenediamine for 10 min, liquid ammonia for 3 h, pyridine for 5 h, triethylphosphine/acetonitrile for 5 h, sodium borohydride/DMF for 24 h, and stirred with *n*-butyllithium in dry hexane for 12 h under nitrogen. These samples were washed and dried with methanol, acetone, and diethyl ether. In all cases, the recovered material consisted primarily of the initial material, $Cs_2Sn_3S_7{\cdot}^1/_2S_8$. A light-brown residue was recovered from the 3 h liquid ammonia leach which was analyzed through SEM-EDS to be $Cs_{1.1}Sn_{2.9}S_7$. Accounting for low cesium content, this analyzed formula is very close to that of the phase of interest, $Cs_2Sn_3S_7$. Powder XRD showed that this material was amorphous and the Raman spectra showed no distinguishable peaks. When a sample of $Cs_2Sn_3S_7{\cdot}^1/_2S_8$ was leached in ethylenediamine for 3 days, the resultant product was a white powder. SEM-EDS indicated that some particles of the white powder were Cs_2S and that the overall bulk material was close to $Cs_2Sn_3S_7$. The white powder was largely amorphous although a few sharp, but unidentified diffraction peaks were present and the Raman spectrum was also unidentified.

Preliminary ion-exchange reactions using KI and NaI solids and KI/CH_3CN and NaI/CH_3CN solutions showed some promise. SEM-EDS indicated that approximately 10% of the Cs^+ cations were exchanged for K^+ when small yellow-green crystals of $Cs_2Sn_3S_7{\cdot}^1/_2S_8$ was submerged in KI/CH_3CN solution at room temperature for three days. Ion exchange was also observed using NaI solid, but the phase identity was changed.

Conclusion

The $Cs_2Sn_3S_7{\cdot}^1/_2S_8$ was formed using the molten polychalcogenide flux synthetic technique and has a framework which is identical to that of compounds previously reported which have only been synthesized through methanothermal and hydrothermal techniques at temperatures below about 160 °C, in some cases requiring the presence of organic templates to form. In analogy, one might say that $Cs_2Sn_3S_7{\cdot}^1/_2S_8$ forms at temperatures up to 500 °C under "polysulfothermal conditions" using S_8 molecules as a template. This material was investigated as a possible microporous tin chalcogenide because it appeared likely that a neutral S_8 species should be easily abstracted. Although this possibility has not been completely ruled out, it now appears unlikely.

The results presented here suggest that the utility of the molten polychalcogenide flux method for synthesis of novel materials is not yet fully exploited and highlights the unique reactivity characteristics of polychalcogenide fluxes. The trapping of S_8 in a metal–sulfide network during framework assembly may not be unique to $Cs_2Sn_3S_7{\cdot}^1/_2S_8$. Encapsulation of other ring sizes,

including polymeric sulfur, may be achievable in various structural frameworks, if the right polysulfide flux conditions are identified.

Acknowledgment. Financial support from the National Science Foundation CHE-9-24102 (Chemistry Research Group) is gratefully acknowledged. The X-ray instrumentation used in this work was purchased in part with funds from the National Science Foundation (CHE-89-08088). This work made use of the SEM facilities of the Center for Electron Optics at Michigan State University. M.G.K. is an A. P. Sloan Foundation, and a Camille and Henry Dreyfus Teacher Scholar, 1993–95.

Supporting Information Available: Table of anisotropic thermal parameters (1 page) calculated and observed X-ray single crystal structure factors (32 pages). Ordering information is given on any current masthead page.

CM950181H